Light-Emitting Tunneling Nanostructures Based on Quantum Dots in a Si and GaAs Matrix

V. G. Talalaev[a, d]^, **A. A. Tonkikh**[a], **N. D. Zakharov**[a], **A. V. Senichev**[a, c], **J. W. Tomm**[b], **P. Werner**[a],
B. V. Novikov[c], **L. V. Asryan**[f], **B. Fuhrmann**[e], **J. Schilling**[d, e], **H. S. Leipner**[d, e],
A. D. Bouraulev[g, h], **Yu. B. Samsonenko**[g, i], **A. I. Khrebtov**[g], **I. P. Soshnikov**[g, h], and **G. E. Cirlin**[g, i]

[a] *Max-Planck-Institut für Mikrostrukturphysik, Weinberg 2, 06120 Halle (Saale), Germany*
^ *e-mail: talalaev@mpi-halle.mpg.de*
[b] *Max-Born-Institut für Nichtlineare Optik und Kurzzeitspektroskopie, Max-Born-Strasse 2a, 12489 Berlin, Germany*
[c] *Fock Institute of Physics, St. Petersburg State University, ul. Ul'yanovskaya 1, Petrodvorets, St. Petersburg, 198504 Russia*
[d] *Martin-Luther-Universität Halle-Wittenberg, ZIK SiLi-nano, 06120 Halle, Germany*
[e] *Martin-Luther-Universität, IZM, 06120 Halle, Germany*
[f] *Virginia Polytechnic Institute and State University, Blacksburg, Virginia 24061, USA*
[g] *St. Petersburg Academic University, Nanotechnology Research and Education Centre,
Russian Academy of Sciences, ul. Khlopina 8/3, St. Petersburg, 194021 Russia*
[h] *Ioffe Physical–Technical Institute, Russian Academy of Sciences, ul. Politekhnicheskaya 26, St. Petersburg, 194021 Russia*
[i] *Institute for Analytical Instrumentation, Russian Academy of Sciences, Rizhskii pr. 26, St. Petersburg, 190103 Russia*
Submitted April 25, 2012; accepted for publication April 25, 2012

Abstract—InGaAs/GaAs and Ge/Si light-emitting heterostructures with active regions consisting of a system of different-size nanoobjects, i.e., quantum dot layers, quantum wells, and a tunneling barrier are studied. The exchange of carriers preceding their radiative recombination is considered in the context of the tunneling interaction of nanoobjects. For the quantum well–InGaAs quantum dot layer system, an exciton tunneling mechanism is established. In such structures with a barrier thinner than 6 nm, anomalously fast carrier (exciton) transfer from the quantum well is observed. The role of the above-barrier resonance of states, which provides "instantaneous" injection into quantum dots, is considered. In Ge/Si structures, Ge quantum dots with heights comparable to the Ge/Si interface broadening are fabricated. The strong luminescence at a wavelength of 1.55 μm in such structures is explained not only by the high island-array density. The model is based on (i) an increase in the exciton oscillator strength due to the tunnel penetration of electrons into the quantum dot core at low temperatures ($T < 60$ K) and (ii) a redistribution of electronic states in the $\Delta_2 - \Delta_4$ subbands as the temperature is increased to room temperature. Light-emitting diodes are fabricated based on both types of studied structures. Configuration versions of the active region are tested. It is shown that selective pumping of the injector and the tunnel transfer of "cold" carriers (excitons) are more efficient than their direct trapping by the nanoemitter.

DOI: 10.1134/S1063782612110218

1. INTRODUCTION

For the most part, in the development of modern optoelectronics, silicon Si and gallium arsenide GaAs are used as substrates, which is connected with the possibility of chip integration of the optical and electronic components. The development of light-emitting elements based on structures with zero-dimensional nanoclusters, i.e., quantum dots (QDs), has a great number of advantages: tunable emission wavelength, thermal stability, and others [1]. Modern optical-fiber communication systems operate using transmission windows at wavelengths of 1.3 and 1.55 μm. The emitting active medium can be adapted to this spectral region using Ge QD arrays in a Si matrix and

InAs QD arrays in a GaAs matrix. Up to now, the problem has been the low efficiency of carrier trapping at QD states [2]. A partial solution to the problem for InGaAs/GaAs structures was found by placing the QD layer in an external quantum well (QW) (DWELL structures), which resulted in more efficient carrier collection in the recombination region and simultaneously shifted emission to an actual wavelength of 1.3 μm due to a decrease in the size quantization level in the InGaAs QD [3]. However, the high density of excited states in DWELL structures reduces the population efficiency of the QD ground state and the internal emission efficiency at the operating wavelength. For Ge/Si structures, the trapping problem is exacer-

bated by the low efficiency of carrier recombination, since the Ge/Si interface belongs to type II: the hole is localized at the Ge QD, and the electron is in the Si layer [4, 5]. Due to the insignificant conduction-band offset, electrons are concentrated at local minima which appear, as a rule, near the QD–Ge/spacer–Si interface due to Coulomb attraction to the QD and elastic stresses [6–8]. The recombination efficiency problem in the Ge/Si system is solved by "pulling" the electron wave function from the Si layer to the Ge QD [7, 9, 10]. Against the background of solution of the above problems, theoretical and experimental studies appeared [11, 12], in which QD and QW layers were separated by a barrier layer; these structures were called hybrid tunneling (injection) structures (HT-structures), since they combine two nanoobjects with different dimensions, 2D (QW) and 0D (QD). Such structures immediately became of special interest in designing the active region of diode lasers. Due to spatial separation of the carrier injector (QW) and light emitter (QD) in them, a new degree of freedom in the active region's design appeared, hence, it became possible to "fit" the QW and QD energy spectra to each other. It is expected that carrier "cooling" in the QW and their direct tunneling to the QD ground state will significantly lower the internal loss, diffusion capacitance, and threshold current, and will increase the response rate and differential efficiency of laser diodes [13, 14].

The emission efficiency of HT-structures is based on the sum of advantages of individual elements of the active region [15]: (i) the large QW trapping cross section and capacitance; (ii) high thermal stability of QD emission; (iii) the efficient carrier exchange between QW and QDs. The last component is associated with tunneling whose features for the QW–QD pair have not been adequately studied [16].

Taking into account these trends, in this work, we attempted to use HT-structures as the active elements of light-emitting diodes based on Si and GaAs. The paper is organized as follows. First, we present new data on InGaAs HT-structures, associated with determination of the tunneling mechanism during the transition from low temperatures to room temperature. In the second part of the paper, we present the latest results on Ge/Si HT-structures in which the efficient emission of small-size Ge QDs was observed near 1.55 μm. For both HT-structure types, general tunneling features were established. At the end of the paper, we use these data to optimize the active region of light-emitting diodes based on HT-structures.

## 2. SAMPLES AND EXPERIMENTAL DETAILS

The samples were grown by molecular-beam epitaxy GaAs (100) and Si (100) substrates. The *active region* consisted of an InAs/GaAs or Ge/Si HT-structure. In the *test samples*, the active region was enclosed in an undoped GaAs or Si *i*-cladding (buffer and cap,

respectively). In the former case, the active region included: a carrier *injector*, i.e., a two-dimensional $In_{0.15}Ga_{0.85}As$ QW 11 nm thick, and a light *emitter*, i.e., a layer of InAs QDs self-assembled from an InAs layer 0.6 nm thick at a temperature of 485°C. The injector and emitter were separated by a GaAs *spacer* whose thickness was set from 2 to 11 nm. For research purposes, two series of test samples were grown: *reference* HT-structures in which the active layer sequence was ordinary (direct) in the QW-spacer-QD growth direction, and *inverse* HT-structures in which the reverse sequence of QD layers, i.e., QD–spacer–QW, was for the first time implemented. In the case of Ge/Si structures, the active region consisted of several layers of self-assembled Ge QDs (light emitter). The thickness of the germanium deposited at a temperature of 600°C was varied from 0.8 to 1.6 nm. The Ge QD layers were separated by Si spacer layers (electron injector) whose thickness was varied from 3 to 20 nm. The specific feature of Ge/Si HT-structure epitaxy was the deposition of an antimony monolayer Sb at various growth stages: before Ge-QD formation (SQD) and above the Ge QDs (LQD). For all series, "control" samples were grown: one of two layers (QW or QD) for InGaAs/GaAs and one QD layer or the absence of an Sb monolayer for Ge/Si.

Light-emitting *p–i–n* diodes were fabricated on doped *p*-type substrates. The active region was formed based on the principles stated above for the test samples. Within the *i*-claddings, limiters, i.e., composite $Al_{0.3}Ga_{0.7}As$ barriers or short-period Ge/Si gratings, for confining injected carriers in the active region (electron confinement) were grown. Outside the *i*-claddings, a *p*-type buffer (*p*-emitter) and an *n*-type cap (*n*-emitter) doped to a concentration of 10^{19} cm^{-3} were arranged. Since measurements were restricted to the subthreshold mode, the light wave in the structures was not specially limited. A mesa structure 1.4 mm in diameter with contact layers was formed by photolithography, reactive etching, and metallization. The fabricated chip was placed into a TO-39 package and was soldered using a gold wire. The diameter of the light-emitting window in the chip was 0.8 mm.

The structural properties of the grown HT-structures were studied by transmission electron microscopy (TEM), by both the dark-field diffraction contrast technique and high-resolution TEM, using Phillips CM20 and JEM 4010 microscopes, respectively. The germanium concentration profiles were measured using a TITAN 300/80 electron microscope.

The steady-state photoluminescence (PL) was excited by an argon laser line at 488 nm (2.54 eV). The excitation density was 50 W cm^{-2}. The spectra were measured using an Edinburgh Instr. cooled germanium photodetector interfaced with a 0.5-meter Acton Research Corp. (ARC) monochromator. All spectra of steady-state PL were corrected to the spectral sensitivity of the measuring circuit. The PL kinet-
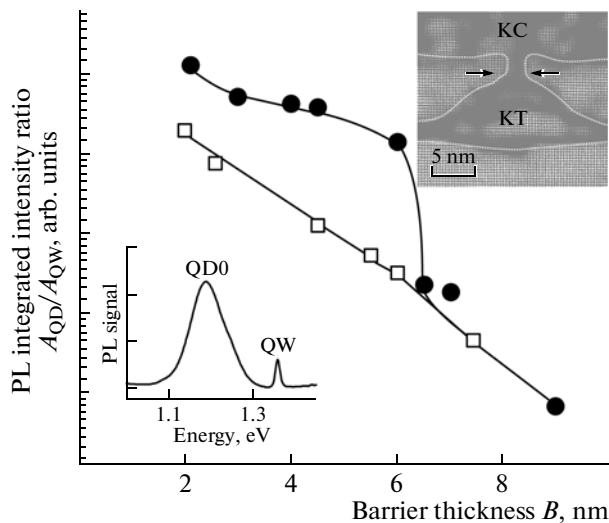
Fig. 1. Ratio of integrated intensities of the QD0 and QW PL bands as a function of the barrier thickness in inverse (circles) and reference (squares) InGaAs/GaAs HT-structures. The lower inset shows the typical PL spectrum for an inverse structure. The upper inset shows TEM images of the region of the inverse HT-structure with a barrier thickness of 3 nm, obtained in the high-resolution mode. The contour is drawn over the contrast boundary corresponding to an approximate indium content of 15%. The arrows indicate the nanobridge connecting the QD top with the QW lower boundary.

ics of the InGaAs structures was studied with a time resolution of 10 ps upon excitation by a Spectra Physics pulsed laser: the pulse repetition rate and duration were 82 MHz and 100 fs, and the photon energy was 1.6 eV (785 nm). The PL signal was synchronously detected by a Hamamatsu streak camera positioned at the ARC monochromator output. The PL kinetics of the Ge/Si structures was studied with a time resolution of 3 ns upon excitation by pulses from a Light Conversion laser system: the frequency and duration were 1 kHz and 200 fs, the photon energy was 2.4 eV (515 nm). At the ARC monochromator output, the signal was measured by a Hamamatsu photomultiplier using an Agilent Tech oscilloscope. The pulse excitation density was 5×10^{11} photon cm^{-2}. The PL measurements were performed in optical cryostats in the temperature range from 5 to 300 K. The electroluminescence (EL) was measured at room temperature in the pulsed current mode with a period of 60 ms and a duty ratio of 1 : 2. The pulse amplitude was tuned by a Thorlabs generator for laser diodes.

3. TRANSMISSION ELECTRON MICROSCOPY AND PHOTOLUMINESCENCE OF InGaAs/GaAs HT-STRUCTURES

Based on TEM statistical analysis, a characteristic barrier B between the QD top and QW layer was determined for each test sample. The two series of nine samples had various sets of barrier thicknesses B. The

HT-structures with a direct layer sequence were presented by a set with B from 1.5 to 10 nm. The series of inverse HT-structures had barriers from 2.0 to 9.0 nm thick. The average error did not exceed 0.5 nm. The TEM analysis also yielded the characteristic sizes of the QDs, i.e., a height of 4 nm and a base of 18 nm. The QD array density was 5×10^{10} cm^{-2}. Analysis of the TEM image contrast showed that the indium content in the QD is $x = 0.6$ due to interdiffusion, while it remains about 0.15 in the 11-nm QW.

In a number of inverse HT-structures, quasi-point contacts were found between the QD tops and the QW lower boundary, which was not observed in the reference series. This conclusion was confirmed by high-resolution TEM data (see the inset in Fig. 1). The detected contacts were shaped close to a cylinder 2 nm in diameter, had varied composition close to that of the QW, and were called nanobridges [17]. The nanobridges were detected in the inverse HT-structures with thin barriers, $B < 6$ nm.

In [17], we found that inversion of the sequence of QW–QD layers separated by a thin barrier results in anomalously fast tunneling between them. This effect was attributed to nanobridge formation. In this work, we continue to study the effect of nanobridges on the tunneling and radiative properties of HT-structures.

The typical spectrum of the stationary PL of the HT-structure consisted of a broad band QD0 of the quantum dot and a narrow peak QW of the quantum well (see the inset in Fig. 1). The ratio of the integrated PL intensities (A) in the QD0 and QW bands depended on the barrier thickness, as shown in Fig. 1. In the region of thin barriers ($B \leq 6$ nm), the dependences $A_{QD0}/A_{QW}(B)$ differed appreciably for the direct and inverse layer sequences. The ratio A_{QD0}/A_{QW} reflects the balance of carrier recombination and transport in the HT-structures; in the case at hand, the role of the QW in QD emission.

The PL kinetic profiles exhibited high sensitivity to the barrier thickness. The PL decay time in the QW band and the PL rise time in the QD0 band correlated, i.e., these times were shorter for thin barriers. The time τ_T of tunneling between QWs and QDs was determined by comparing the PL time profiles and solutions to the balance equations for carriers in QWs and QDs [18]. The extracted data are shown in Fig. 2 for both series of InGaAs/GaAs HT-structures in the form of the dependences $\tau_T(B)$ in the semilogarithmic scale [19, 20]. In the region of "thick" barriers ($B \geq 6$ nm), the dependences $\tau_T(B)$ for both series were identical. In the case of thin barriers, the tunneling time in the inverse HT-structures deviated from the exponential dependence and came closer to the instrumental time resolution (10 ps). Noteworthy is also the correlation of the barrier dependences in Figs. 1 and 2.

As the temperature increases to room temperature, the time decay of the QW PL in the HT-structures with

Tunneling time τ_T, ps
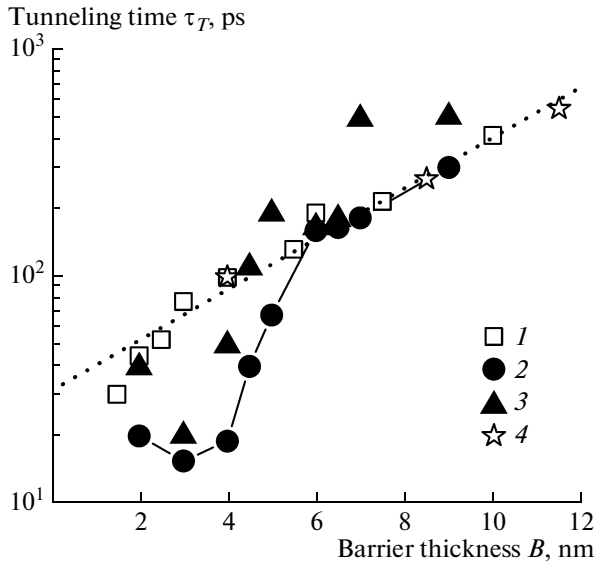
Fig. 2. Tunneling time τ_T as a function of the barrier thickness B between the QW and QD: (*1*) reference series of HT-structures, (*2*) inverse series at $T = 5$ K, and (*3*) the same series at room temperature. The values of τ_T were determined by analyzing the QW PL decay upon excitation into the GaAs matrix. (*4*) Data on QD–QD tunneling [19, 20]. The dotted line is the WKB approximation.

PL signal, arb. units

Fig. 3. PL decay in the QW band of the inverse HT-structures with a barrier $B = 7$ nm, measured at temperatures of (*1*) 100, (*2*) 160, (*3*) 200, (*4*) 230, (*5*) 260, and (*6*) 300 K. Excitation into the GaAs matrix.
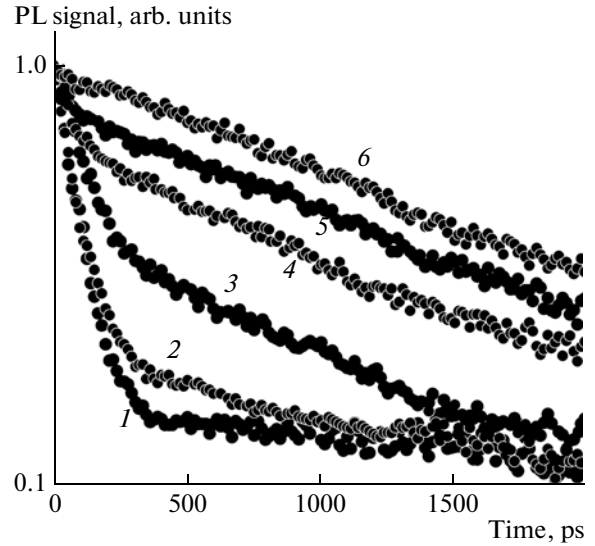
thick barriers was transformed, as shown in Fig. 3. It is clearly seen that a new slower component appears at $T \geq 160$ K. Against its background, the fast component disappears from the PL spectrum at $T = 300$ K. This did not occur in the inverse HT-structures with thin barriers. As their temperature increases, the QW PL decay remained rapid in the entire temperature range of 5–300 K.

4. TUNNELING IN InGaAs/GaAs HT-STRUCTURES

The experimental dependence $\tau_T(B)$ was compared with the exponent $\tau_T(B) = c_0 \exp(c_1 B)$ given by the semiclassical approximation for an asymmetric QW pair (Wentzel–Kramers–Brillouin (WKB) model) and is written in the explicit form [21–23] as

$$\tau_T = L \frac{[U + E(m_B^*/m_W^* - 1)]^2 \sqrt{2m_W^*}}{16 E^{3/2} (U - E)(m_B^*/m_W^*)} \\ \times \exp\left[\frac{2B}{\hbar}\sqrt{2m_B^*(U - E)}\right]. \quad (1)$$

For the reference series, the dependence $\tau_T(B)$ remains exponential almost in the entire B range (Fig. 2). For the inverse HT-structures, the dependence $\tau_T(B)$ deviates from the WKB model for thin barriers ($B < 6$ nm). It is noteworthy that the linear

regions of $\log \tau_T(B)$ for both series are almost identical to the dependence $\tau_T(B)$ for pair InGaAs QDs (Fig. 2).

However, all three cases have numerical values for the coefficients c_0 and c_1, which are far from that given by the model (1) for any carrier type, including excitons. This is grounds to assume that it is not the difference in the dimensions of the nanosystem components, but the existence of quasi-zero-dimensional QDs as one of the components that makes the semiclassical approach using formula (1) inapplicable, and requires special calculations of the tunneling time for QD–QD and QW–QD systems.

Since a comparison of the experimental and calculated dependences $\tau_T(B)$ does not unambiguously answer the question regarding the type of carriers tunneling in HT-structures, let us turn to other experimental facts [17].

(i) In the PL excitation spectra, the signal from the QW was always shaped as a narrow peak, instead of a step characteristic of the density of states in the QW.

(ii) Selective excitation of the QW resulted in QD0 PL, while excitation of the control sample with the same energy (without a QW) did not yield a PL signal.

(iii) The tunneling times τ_T extracted from the PL decay in the QW (injector) band and from the QD0 time profile (recipient) were identical.

(iv) The barrier dependences of the tunneling time (Fig. 2) and the relative intensity of the QD0 and QW bands (Fig. 1) are formed by common mechanisms.

These data allow the conclusion that the excitation transfer between the QW and QDs in HT-structures is performed in correlation with carriers of both signs, i.e., by the electron–hole pair (exciton). The strong
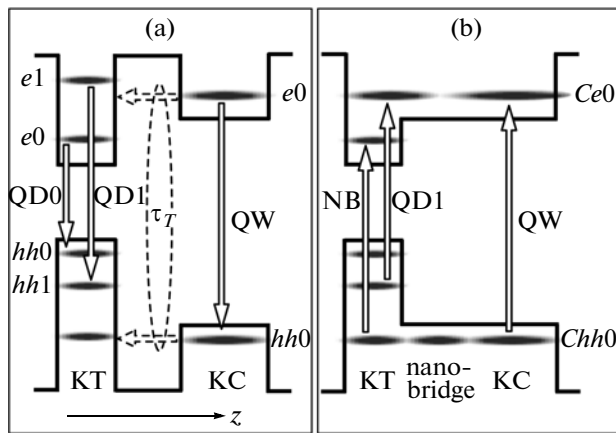
Fig. 4. Energy level diagram for two types of inverse InGaAs/GaAs HT-structures: (a) without a nanobridge (barrier thickness $B \geq 6$ nm) and (b) with a nanobridge (barrier thickness $B < 6$ nm). Optical transitions correspond to the (a) PL and (b) PL excitation modes.

Coulomb correlations characteristic of low-dimensional heterostructures compel us to pay attention to the exciton as one of the main participants of excitation transfer [24]. The most efficient (and most discussed) mechanisms of exciton relaxation in tunnel-coupled structures are exciton tunneling with longitudinal optical (LO) phonon scattering and scattering at interface inhomogeneities [25−28], and also photon exchange and dipole−dipole interaction for thick tunnel barriers [29, 30]. In what follows, we identify the exciton relaxation mechanism in the studied HT-structures.

The relaxation times within the QD were extracted from an analysis of the PL rise time profile in the QD0 band. For the reference series and inverse HT-structures without nanobridges ($B > 6$ nm), the relaxation time was ~1 ns. Such times are typical of acoustic-phonon scattering. Since the criterion $\Delta E_{ex} > 2\hbar\omega_{LO}$ is satisfied for the exciton energy gap in the studied InGaAs/GaAs structures, we assume that exciton tunneling relaxation without nanobridges occurs via the step mechanism [26−28]. The free exciton in the QW is elastically scattered at the interface, donating an electron to the QD. The electron and hole separated by the barrier, but still bound by the Coulomb force, form an indirect exciton. The hole stimulated by the Coulomb interaction tunnels into the QD. In contrast to single-particle tunneling, constraints on this transition, associated with the necessity of LO-photon emission, are relieved due to exciton energy spectrum renormalization ($\Delta E_{ex} > 2\hbar\omega_{LO}$). Subsequent acoustic-phonon scattering completes the exciton transition to the final state in the QD from which radiative recombination QD0 occurs (Fig. 4a).

The direct transition of the direct exciton from the QW to the QD with LO-photon emission, proposed in [31], could be an alternative mechanism for exciton relaxation in inverse HT-structures. However, for such a mechanism to be implemented, strong tunnel coupling of potential wells is required. It is clear that this requirement is satisfied by structures in which QWs and QDs are coupled by nanobridges. The TEM studies showed that these point contacts appear during inversion of the sequence of layers separated by a thin spacer. The TEM data showed that nanobridges are formed due to elastic stresses at the QD top, which cause indium atom diffusion during spacer growth, which results in the formation of indium-rich channels between the QDs and the QW.

Manifestations of nanobridges in the PL of inverse HT-structures with $B < 6$ nm are the following effects.

(i) Deviation of the dependence $\tau_T(B)$ from the exponential function $c_0\exp(c_1B)$ and a decrease in the tunneling time τ_T to 15 ps (Fig. 2);

(ii) a decrease in the relaxation time within the QD from 1 ns to 40 ps [32];

(iii) an increase in the PL intensity in the QD band (Fig. 1); and

(iv) a narrow NB line in the PL excitation spectrum [33] (Fig. 4b).

We proceed from the fact that the nanobridge composition is close to that of the QW ($x = 30\%$). This means the local disappearance of the barrier between the well and the QD top. As a result, a single *composite* QW is formed (Fig. 4b). Elimination of the potential barrier by the nanobridge results in the above-barrier interaction of the QW and QD states, similar to Breit−Wigner resonance [34], which is accompanied by interference and hybrid quasi-steady state formation. The common size quantization subband in the composite QW is formed mainly in the conduction band due to the interpenetration of electron wave functions. Since the nanobridge and QD occupy only an insignificant part of the composite QW, the position of the electron subband $Ce0$ and its parameters are predominantly controlled by the parameters of the initial "unperturbed" QW and its ground state $e0$ (Fig. 4).

In contrast to electrons, the interpenetration of heavy-hole wave functions is limited. Therefore, the existence of the nanobridge "perturbs" the hole subsystem to a lesser extent. The situation changes when the nanobridge can have a hole eigenstate [33]. Its resonant interaction with the QW and QD states can cause the formation of a single hole subband $Chh0$ in the composite QW (Fig. 4b). The QD levels appeared out of resonance are controlled by the parameters of the QD itself and the surrounding bulk layer; however, their position can change after formation of the composite QW. These changes will be insignificant for deep levels in the QD, but can turn out to be significant for weakly localized states.

Thus, the nanobridge with the hole eigenstate becomes a factor that can provide "instantaneous"
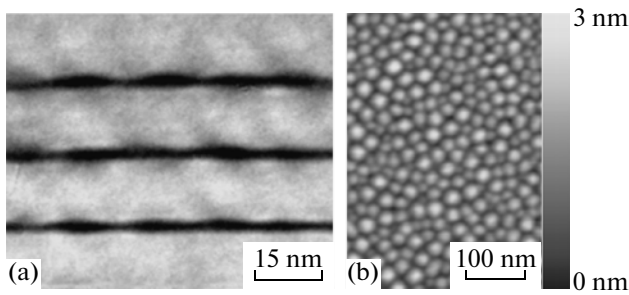
Fig. 5. (a) Dark-field TEM image of the cross section and (b) AFM micrograph of the Ge/Si HT-structures with small SQD QDs. The TEM micrograph is taken in the chemically sensitive reflection (200).


Fig. 6. (a) Local TEM image of the Ge/Si HT-structure with small SQD QDs, made in the stress-sensitive mode. (b) Germanium concentration profiles for three structures: (*1*) small SQD QDs (Sb deposition before QDs); (*2*) LQD QDs (Sb deposition after QDs); the dotted curve *3* corresponds to the control sample grown without Sb.

exciton injection from the QW to the QD. Since the requirement of strong coupling of two potential wells [31] is ideally satisfied in this case, we believe that the exciton in the HT-structure with nanobridges tunnels as a single unit, without the intermediate state of an indirect exciton. The absence of barriers for the electron and hole and the presence of hybrid states makes the transfer "instantaneous" (Fig. 2). Can these factors provide "instantaneous" carrier injection from the QW to the QD during a single-particle transfer, when the exciton does not exist, e.g., at high temperatures?

The binding energy E_B of the direct exciton in the QW, similar to that in the InGaAs−HT-structure, and the indirect exciton (taking into account the dependence of E_B on the barrier thickness) is 6−9 meV [35−37]. Thus, the exciton nature of the tunneling will disappear with increasing temperature. As seen from the temporal PL spectra (Fig. 3), in the HT-structure without nanobridges ($B = 7$ nm) at $T = 160$ K ($kT \approx 14$ meV), the fast component of QW decay begins to be replaced by the slow component which dominates with a time constant of ~500 ps at $T = 300$ K. Thus, single-particle tunneling of carriers occurs instead of the exciton relaxation mechanism.

In the HT-structures with nanobridges, the QW PL decay profiles at low and room temperatures are described by close time constants [32]. Due to the existence of hybrid levels, carrier relaxation in such structures at high temperature is identical to resonant tunneling via excited states with intermediate phonon emission.

Competition between the processes of tunneling from the QW and radiative recombination in the QW leads to correlation of the dependences $A_{QD0}/A_{QW}(B)$ (Fig. 1) and $\tau_T(B)$ (Fig. 2). A decrease in the tunneling time with decreasing barrier thickness provides a gain in the QD0 transition intensity. Comparison with the control sample containing only a QD layer shows that the appearance of the QW in the tunneling vicinity of the QD can increase the relative QD PL intensity by one order of magnitude; the formation of nanobridges can increase this by two orders of magnitude. The
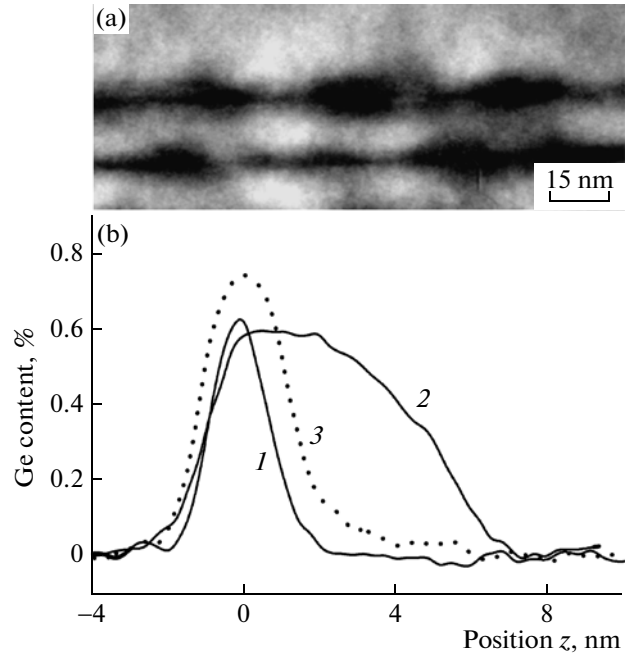
identity of the barrier dependences for the tunneling time (Fig. 2) and PL intensity (Fig. 1) makes it possible to use any one of them as an independent indicator of the presence of nanobridges in the structure.

5. TRANSMISSION ELECTRON MICROSCOPY AND PHOTOLUMINESCENCE OF Ge/Si HT-STRUCTURES

Analysis of the TEM data allowed us to determine the characteristic sizes of the Ge QDs, i.e., the base size L and height h. These parameters of LQD (Sb deposition after QDs) and SQD (Sb deposition before QDs) quantum dots were $L \approx 60$ nm, $h \approx 5$ nm and $L \approx 15$ nm, $h \approx 2.5$ nm, respectively. In the control sample (without Sb), L and h were intermediate. Fabrication of Ge nanoclusters with minimum size (SQD type) but with maximum packing density was the purpose of the technological part of this work. Figure 5 shows the TEM image of such QDs (a) and the atomic-force microscopy micrograph (b). The SQD QD array density was high, ~2 × 10^11 cm^−2. Figure 6 shows the TEM data obtained in two modes sensitive to elastic stresses (b) and the Ge_xSi_{1-x} composition (a). The germanium concentration profiles in the QDs characterize the Ge and Si interdiffusion, which resulted in that the maximum Ge content in the QD core did not exceed 60%, and the interface broadening reached 1.5 nm.
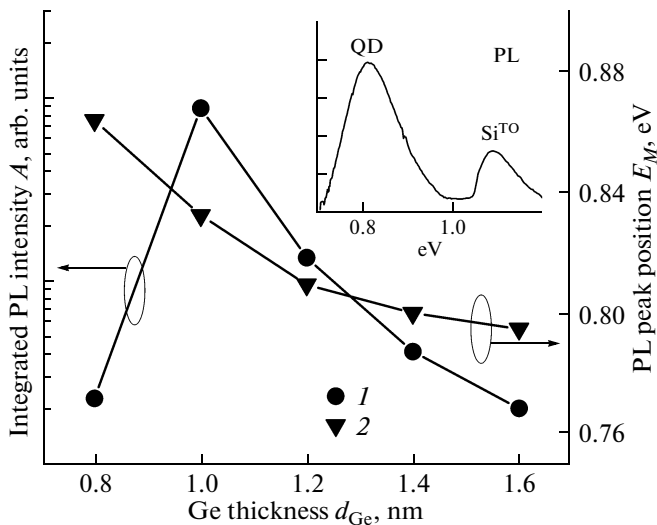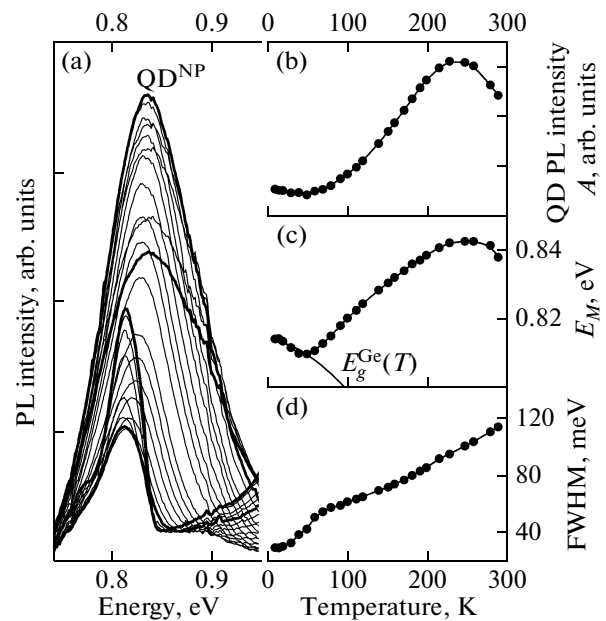
Fig. 7. Effect of the pseudomorphic Ge layer thickness on the QD PL band parameters for Ge/Si HT-structures with one Ge QD layer. (*1*) Integrated PL intensity and (*2*) spectral peak positions. The inset shows the typical spectrum of the Ge/Si HT-structure. All measurements were performed at room temperature.

Fig. 8. (a) Effect of temperature on the PL in the QD band and the temperature dependence of the PL parameters: (b) integrated intensity A, (c) peak position E_M, (d) width FWHM. (a) Bold curves are the contours of the QD band at temperatures of 5, 60, 230, and 290 K. The Ge/Si HT-structure with small SQD QDs ($d_{Ge} = 1$ nm) was measured.

At room temperature and upon optical excitation, radiative recombination in the Ge/Si HT-structures with QDs was characterized by two spectral components: a Si^{TO} PL band of bulk silicon and a broader QD PL band near 1.55 μm (0.8 eV) (see the inset in Fig. 7). The maximum QD PL signal was obtained for the structures with small QDs formed from a Ge layer of the thickness $d_{Ge} = 1$ nm (Fig. 7). The origin of the QD component is indicated by the dependence of its spectral position E_M on the thickness of the deposited germanium d_{Ge} (Fig. 7).

The temperature dependence of the QD band's parameters is shown in Fig. 8. The SQD PL band featured an asymmetric (doublet) structure with an intense non-phonon component (Fig. 8a), nonmonotonic variation of the integrated intensity A (Fig. 8b), and the transition energy E_M at the maximum (Fig. 8c). The full width at half-maximum (FWHM) near $T \approx 60$ K contained a characteristic kink (Fig. 8d). The increase in the QD intensity in the temperature range of 60–230 K is indicative of the fact that, along with the thermal ejection of carriers, there is competitive population of the level involved in the QD optical transition. The "red" deviation of the dependence $E_M(T)$ from the Varshni law for the GeSi system with Ge QDs was previously observed in [9]; however, the "blue" shift in the wide temperature range of 60–230 K was observed for the first time.

6. TUNNELING IN Ge/Si HT-STRUCTURES

The QD PL band results from radiative recombination of the electron–hole pair at the second-type interface, i.e., Ge QD/Si spacer. The nature of this band was determined in numerous studies (see, e.g., [5, 38–41]) based on the band model proposed in [42]. Tensile stresses in the Si layers adjoining the QDs lift the sixfold degeneracy of the conduction band near the Δ-minimum, leading to splitting into Δ_4 and Δ_2 valleys; the latter represents an energy minimum for electrons. In the Ge QD, the Δ_4 valley forms a weak minimum [43]. Compressive stresses that exist there also split the valence band, which is degenerate at the Γ point, into subbands of heavy (hh) and light holes.

Heavy holes are highly localized by Ge islands. Thus, the Δ_2–hh recombination transition is indirect in both real and reciprocal spaces. The weak overlap of the electron and hole wave functions at the interface causes the low efficiency of their recombination. The indirect exciton features a weak oscillator strength. Most studies on overcoming this limitation are reduced to attempts to pull the electron from the Si layer to the Ge/Si interface as much as possible, and to force it to tunnel to the Ge QD [7, 9, 10]. In this regard, of interest is the effect of the germanium thickness (d_{Ge}) on the QD PL intensity (A), shown in Fig. 7. For small SQD QDs obtained from a layer with $d_{Ge} = 1$ nm, the PL intensity is highest within this dependence.

The fabrication of small QDs and the achievement of intense PL become possible due to the deposition of germanium onto the antimony layer [44]. Being an

active surfactant, antimony changes the surface kinetics of Ge adatoms: it shortens the diffusion length, thus preventing QD coarsening. The strongest size effect is achieved when depositing antimony before QD formation. The maximum effect for PL is achieved for seven Ge monolayers (1 nm). How does the QD downsizing result in a strong PL signal at a wavelength of 1.55 μm at room temperature? Two causes seem evident. The effect of PL enhancement with decreasing Ge QD sizes can be associated with an increase in the density of the QD array and with delocalization of the hole state *hh* in reciprocal space. However, these causes do not explain the weak PL at the edge point with $d_{Ge} = 0.8$ nm (Fig. 7).

In this study, we explain this effect by the electron redistribution between the Δ_2 and Δ_4 valleys with decreasing Ge QD sizes. The Ge/Si interface is not perfect (Fig. 6b), but contains a broadening comparable to the total height of the SQD island (1.5 and 2.5 nm, respectively). This is caused by the interdiffusion of Si and Ge atoms during island overgrowth. According to high-resolution TEM data, the core of the small QDs with $x = 60\%$ contains only 3−5 germanium monolayers, i.e., 0.4−0.7 nm.

Mixing of the GeSi material occurs against the background of high stresses appearing near the interface. In the HT-structures with small QDs, tensile stresses are extended in both directions away from the interface, while compressive stresses in the QDs strengthen (Fig. 6a). According to Raman scattering data, the Raman shift of the Ge−Ge LO-mode in small QDs by 7 cm^{-1} is larger than that in the LQD QD. Both factors result in lowering of the Δ_4 subband within the QD, with the result that its final position can become energetically more favorable for electrons of the Δ_2 subband. We attribute the features of the temperature dependence of the PL of HT-structures with small QDs to thermally activated $\Delta_2-\Delta_4$ electronic transitions (Fig. 8). This dependence essentially distinguishes SQD QDs from the small strained Ge QDs grown at low temperatures in [45].

Electrons near small islands are weakly localized and confined by local minima of Δ_2 only at low temperatures ($T < 60$ K). In this temperature range, the QD PL band parameters follow variations in the Ge and Si bands (transition energy E_M) and thermal ejections from shallow wells Δ_2 (integrated intensity A). As the thermal energy increases in the range of 60−230 K, ejections of electrons can be accompanied by their trapping at the Δ_4 subband forming a minimum in the QD. The QD band shifts to high energies. The broadening corresponds to the transition to the valley with a different density of states and a lighter effective mass. The PL intensity increases, since the Δ_4-hh recombination corresponds to type I (direct exciton). At higher temperatures, the recombination type is retained. The valley involved in the QD transition can
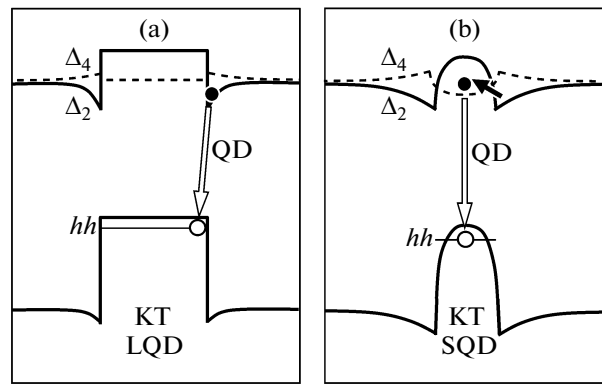

Fig. 9. Model of the band diagram for the Ge/Si HT-structures with (a) LQD and (b) SQD QDs.

be identified by comparing the intensities of the phonon (QD^{OP}) and non-phonon (QD^{NP}) PL components at varied nanocluster sizes [46]. In the case at hand, due to the expected change in the valleys at $T \geq$ 60 K, such a comparison should be performed for two temperature ranges and with a larger number of samples in the series. An indirect indication of the fact that radiative recombination processes are concentrated in small QDs is the lack of dependence of the PL on the spacer thickness which was varied within 3−20 nm. From the temperature dependence of the PL intensity (Arrhenius analysis), the following parameters of the band structure were determined: the energy gap $\Delta_2-\Delta_4$ (~35 meV) and the depth of the Δ_4 minimum in the QD (~50 meV).

Based on these data, using the shape of the Ge concentration profiles (Fig. 6b), we illustrate the proposed model by the schematic diagram in Fig. 9. The local potential wells Δ_2 for electrons near the base and top of small SQD QDs are broadened in comparison with LQD QDs. The tunnel barrier Δ_2 separating them in the QDs is more transparent. Such a situation taking place at low temperatures, $T < 60$ K, is similar to the case of a double QW with a thin potential barrier. The weakly localized electronic states of both wells penetrate in a tunnel manner into the QD core, the electron−hole wave functions are overlapped, and the transition oscillator strength increases. A temperature increase redistributes the electronic states from the Δ_2 subband to the minimum of the Δ_4 subband in the QD and stimulates the transition to the direct exciton. The observed PL quenching at the edge point of the dependence in Fig. 7 ($d_{Ge} = 0.8$ nm) is explained by a decrease in the power of the Δ_4 potential well, which results in its emptying at high temperatures. Thus, within the proposed model, room-temperature excitation relaxation passes from the Si matrix through the Δ_2 valley to the interface and then, via thermally stimulated tunneling, to the Δ_4 valley and the SQD QD core. The model of direct dynamic recombination in the Ge QD with Δ_2 valley filling with electrons was
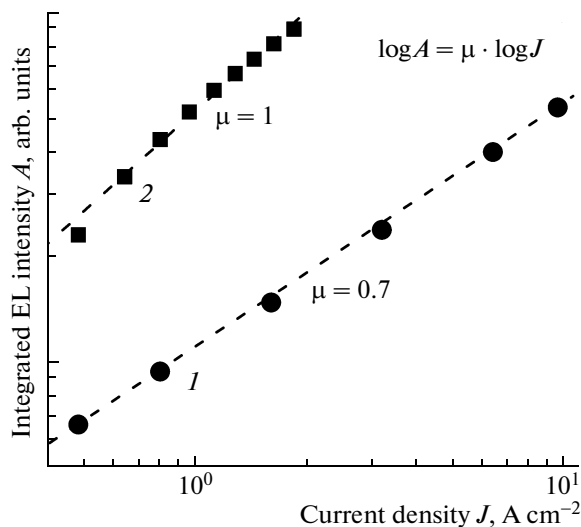
Fig. 10. Room-temperature dependence of the integrated EL intensity for two Ge/Si HT-structures (*1*) with and (*2*) without *i*-claddings.

Fig. 11. Room-temperature current dependence of the relative EL intensity of the QD0 and QW bands for two InGaAs/GaAs HT-structures (*1*) with and (*2*) without nanobridges.
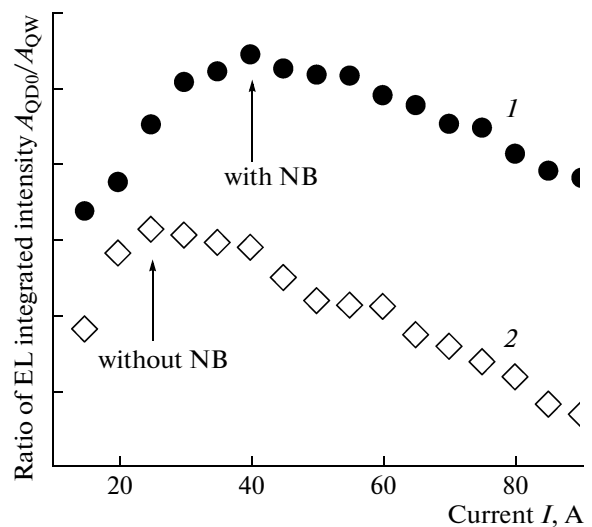
proposed in [47] and applied in [48–50] to ordinary Ge/Si QDs subjected to intense optical pumping.

Time-resolved PL measurements showed that the radiative lifetime in HT-structures with a small SQD QD at room temperature is 50–120 ns. This result is an argument in favor of the proposed mechanism for the transition to the direct exciton, since the characteristic lifetimes of the indirect exciton in the Ge/Si structure are several microseconds [5, 51]. The achieved effect of decreasing the Ge QD size in the Ge/Si HT-structure was used in the present study to develop light-emitting *pin*-diodes with a high external EL efficiency for a Ge/Si system.

7. ELECTROLUMINESCENCE OF HT-STRUCTURES

Of crucial importance for the use of HT-structures in lasers are the parameters of the luminescence under electrical pumping, i.e., electroluminescence (EL). In contrast to the active region, assembling principles and the nature of processes in the outer layers are common for InGaAs/GaAs and Ge/Si HT-structures.

For example, the emission efficiency can be increased by supplementing the active region with *i*-claddings of undoped matrix material. In Fig. 10, we demonstrate this for the Ge/Si HT-structure. As the current density J increases, the EL intensity growth factor μ for the QD band in structures with *i*-claddings is unity, whereas $\mu < 1$ in structures without *i*-claddings. This effect is probably caused by the partial thermalization of "hot" carriers in *i*-claddings, injected by *n*- and *p*-emitters. Measurements for light-emitting diodes based on Ge/Si HT-structures with small QDs showed that the currently achievable external quantum efficiency is up to 0.8×10^{-4}, which is an absolute record for Ge/Si structures with Ge QDs at a wavelength of 1.55 μm at room temperature [9, 52, 53].

The design of the electron confinement region was the subject of an independent study. Carrier spreading from the active region was bounded by additional barriers within the *i*-claddings. We proceeded from two evident principles providing the confinement efficiency.

(i) The closest approach of the barriers to the active region; and

(ii) the maximum selectivity of the barriers with respect to opposite-sign carriers.

In this study, these principles were tested with the following results.

(i) To prevent defect formation and distortion of the spectra of the active nanoobjects, it is reasonable to move the barriers further from the active region (by 20 nm in this study); and

(ii) to simplify the growth technology of the *p–i–n* structures, selective barriers can be replaced by composite nonselective ones without significant losses in its advantages.

Figure 11 shows the results of a comparative study of room-temperature InGaAs/GaAs HT-structures arranged in the *i*-region, formed according to the above principles. The relative intensities of A_{QD0}/A_{QW} EL bands for the HT-structures with and without nanobridges were compared. The presence of nanobridges which enhance tunneling between the QWs and QDs provides a gain in the EL intensity and makes the A_{QD0}/A_{QW} positive slope region more extensive. This result indicates the high efficiency of the electrical pumping of HT-structures with nanobridges and offers prospects for their use in laser devices. "Instan-

taneous" injection can appear to be a new mechanism stimulating the development of efficient light emitters. The formation of channels of direct carrier exchange through InGaAs nanobridges (Fig. 4b) can simplify the scheme of the double tunnel–injection structure proposed in [54, 55] for high-power diode lasers with high thermal stability. In the HT-structure with nanobridges, one QW can provide two-particle pumping of the QD, and the second QW can become unnecessary. A decrease in the number of precision layers in the heterostructures makes laser fabrication on their basis more producible.

Thus, the benefits of the developed HT-nanostructures are confirmed by the EL studies on light emitting chips with an optimized *i*-region. Among these are: for InGaAs/GaAs structures, the presence of nanobridges in the case of the inverse sequence of layers with barriers thinner than 6 nm; for Ge/Si structures, small QDs with a nanoscale interface. Optimization of the *i*-region consists of the development of "cooling" *i*-claddings with additional barriers for efficient electron confinement.

8. CONCLUSIONS

The transport and radiative properties of InGaAs/GaAs and Ge/Si HT-structures with QDs were studied. The tunneling properties of the structures were studied by TEM and PL methods. The exciton nature of the tunneling in the InGaAs QD–QW system at low temperatures was experimentally determined ($T < 160$ K). For such a layer sequence (in contrast to the QW–QD pair) for thin tunnel barriers (<6 nm), ultrafast carrier (exciton) exchange for the wide temperature range 5–300 K was detected. The dependence of the tunneling time for such HT-structures does not obey the exponential law and is explained by "instantaneous" injection through nanobridges closing QD and QW tops and with a hole eigenstate. In Ge/Si HT-structures with small QDs, intense emission at a wavelength of 1.55 μm was observed. The sizes of the germanium islands were comparable to the interface broadening. A model that adequately explains the experimental data for the Ge/Si HT-structures was proposed: the dependences of the PL intensity on the Ge layer thickness and measurement temperatures, the radiative lifetime of the direct exciton, and Raman scattering. It is based on the increase in the exciton oscillator strength due to the tunneling penetration of electrons into the QD core at low temperatures ($T < 60$ K); the redistribution of the electronic states in the Δ_2–Δ_4 subbands as the temperature increases to room temperature. Based on the studied HT-structures of both types, light-emitting diodes were fabricated and active-region design types were tested.

REFERENCES

1. N. Kirstaedter, N. N. Ledentsov, M. Grundmann, D. Bimberg, V. M. Ustinov, S. S. Ruvimov, M. V. Maximov, P. S. Kop'ev, Zh. I. Alferov, U. Richter, P. Werner, U. Gösele, and J. Heydenreich, Electron. Lett. **30**, 1416 (1994).

2. A. E. Zhukov, *Lasers Based on Semiconductor Nanostructures* (Elmor, St.-Petersburg, 2007) [in Russian].

3. A. E. Zhukov, A. R. Kovsh, A. Yu. Egorov, N. A. Maleev, V. M. Ustinov, B. V. Volovik, M. V. Maksimov, A. F. Tsatsul'nikov, N. N. Ledentsov, Yu. M. Shernyakov, A. V. Lunev, Yu. G. Musikhin, N. A. Bert, P. S. Kop'ev, and Zh. I. Alferov, Semiconductors **33**, 153 (1999).

4. M. M. Rieger and P. Vogl, Phys. Rev. B **48**, 14276 (1993).

5. S. Fukatsu, H. Sunamura, Y. Shiraki, and S. Komiyama, Appl. Phys. Lett. **71**, 258 (1997).

6. V. Ya. Aleshkin, N. A. Bekin, N. G. K. Kalugin, Z. F. Krasil'nik, A. V. Novikov, and V. V. Postnikov, JETP Lett. **67**, 48 (1998).

7. O. G. Schmidt, K. Eberl, and Y. Rau, Phys. Rev. B **62**, 16715 (2000).

8. A. V. Dvurechenskii and A. I. Yakimov, Semiconductors **35**, 1095 (2001).

9. V. G. Talalaev, G. E. Tsyrlin, A. A. Tonkikh, N. D. Zakharov, P. Werner, U. Gösele, J. W. Tomm, and T. Elsaesser, Nanoscale Res. Lett. **1**, 137 (2006).

10. A. V. Novikov, M. V. Shaleev, A. N. Yablonskii, O. A. Kuznetsov, Yu. N. Drozdov, D. N. Lobanov, and Z. F. Krasilnik, Semicond. Sci. Technol. **22**, S29 (2007).

11. L. V. Asryan and S. Luryi, IEEE J. Quant. Electron. **37**, 905 (2001).

12. L. F. Register, C. Wanqiang, X. Zheng, and M. Stroscio, Int. J. High Speed Electron. Syst. **12**, 239 (2001).

13. P. Bhattacharya, S. Ghosh, S. Pradhan, J. Singh, Z. K. Wu, J. Urayama, K. Kim, and T. B. Norris, IEEE J. Quant. Electron. **39**, 952 (2003).

14. Z. Mi, P. Bhattacharya, and S. Fathpour, Appl. Phys. Lett. **86**, 153109 (2005).

15. V. P. Evtikhiev, O. V. Konstantinov, A. V. Matveentsev, and A. E. Romanov, Semiconductors **36**, 74 (2002).

16. G. Sek, P. Poloczek, P. Podemski, R. Kudrawiec, J. Misiewicz, A. Somers, S. Hein, S. Höfling, and A. Forchel, Appl. Phys. Lett. **90**, 081915 (2007).

17. V. G. Talalaev, J. W. Tomm, N. D. Zakharov, P. Werner, U. Gösele, B. V. Novikov, A. S. Sokolov, Yu. B. Samsonenko, V. A. Egorov, and G. E. Tsyrlin, Appl. Phys. Lett. **93**, 031105 (2008).

18. V. G. Talalaev, A. V. Senichev, B. V. Novikov, J. W. Tomm, T. Elsaesser, N. D. Zakharov, P. Werner, U. Gösele, Yu. B. Samsonenko, and G. E. Tsyrlin, Semiconductors **44**, 1050 (2010).

19. Yu. I. Mazur, Zh. M. Wang, and G. G. Tarasov, Phys. Rev. B **71**, 235313 (2005).

20. V. G. Talalaev, J. W. Tomm, A. S. Sokolov, I. V. Shtrom, B. V. Novikov, A. Winzer, R. Goldhahn, G. Gobsch, N. D. Zakharov, P. Werner, U. Gösele, G. E. Tsyrlin, A. A. Tonkikh, V. M. Ustinov, and G. G. Tarasov, J. Appl. Phys. **100**, 083704 (2006).

21. T. Tada, A. Yamaguchi, T. Ninomiya, H. Uchiki, T. Kobayashi, and T. Yao, J. Appl. Phys. **63**, 5491 (1988).

22. M. Nido, M. G. W. Alexander, and W. W. Ruehle, Appl. Phys. Lett. **56**, 355 (1990).

23. J. N. Zeng, I. Souma, Y. Amemiya, and Y. Oka, J. Surf. Anal. **3**, 529 (1997).

24. S. V. Zaitsev, A. S. Brichkin, P. S. Dorozhkin, and G. Bacher, Semiconductors **42**, 813 (2008).

25. I. Lawrence, S. Haacke, H. Mariette, W. W. Rühle, H. Ulmer-Tuffigo, J. Cibert, and G. Feuillet, Phys. Rev. Lett. **73**, 2131 (1994).

26. S. Ten, F. Henneberger, M. Rabe, and N. Peyghambarian, Phys. Rev. B **53**, 12637 (1996).

27. D. A. Mazurenko and A. V. Akimov, Phys. Solid State **43**, 752 (2001).

28. S. V. Zaitsev, A. S. Brichkin, Yu. A. Tarakanov, and G. Bacher, Phys. Status Solidi B **247**, 353 (2010).

29. A. Tomita, J. Shah, and R. S. Knox, Phys. Rev. B **53**, 10793 (1996).

30. S. K. Lyo, Phys. Rev. B **62**, 13641 (2000).

31. F. C. Michl, R. Winkler, and U. Roessler, Solid State Commun. **99**, 13 (1996).

32. V. G. Talalaev, A. V. Senichev, B. V. Novikov, J. W. Tomm, L. V. Asryan, N. D. Zakharov, P. Werner, A. D. Buravlev, Yu. B. Samsonenko, A. I. Khrebtov, I. P. Soshnikov, and G. E. Tsyrlin, Vestn. SPb. Univ. (2012, in press).

33. A. V. Senichev, V. G. Talalaev, J. W. Tomm, B. V. Novikov, P. Werner, and G. E. Tsyrlin, Phys. Status Solidi (RRL) **5**, 385 (2011).

34. Ch. S. Kim, A. M. Satanin, and V. B. Shtenberg, Semiconductors **36**, 539 (2002).

35. R. C. Iotti and L. C. Andreani, Semicond. Sci. Technol. **10**, 1561 (1995).

36. M. Bayer, S. N. Walck, and T. L. Reinecke, Phys. Rev. B **57**, 6584 (1998).

37. I. Galbraith and G. Duggan, Phys. Rev. B **40**, 5515 (1989).

38. H. Sunamura, S. Fukatsu, N. Usami, and Y. Shiraki, J. Cryst. Growth **157**, 265 (1995).

39. O. G. Schmidt, O. Kienzle, Y. Hao, K. Eberl, and F. Ernst, Appl. Phys. Lett. **74**, 1272 (1999).

40. K. Eberl, O. G. Schmidt, R. Duschl, O. Kienzle, E. Ernst, and Y. Rau, Thin Solid Films **369**, 33 (2000).

41. A. V. Novikov, D. N. Lobanov, A. N. Yablonskii, Y. N. Drozdov, N. V. Vostokov, and Z. F. Krasilnik, Physica E **16**, 467 (2003).

42. T. Baier, U. Mantz, K. Thonke, R. Sauer, F. Schäffler, and H.-J. Herzog, Phys. Rev. B **50**, 15191 (1994).

43. M. El Kurdi, S. Sauvage, G. Fishman, and P. Boucaud, Phys. Rev. B **73**, 195327 (2006).

44. A. Tonkikh, N. Zakharov, V. Talalaev, and P. Werner, Phys. Status Solidi (RRL) **4**, 224 (2010).

45. T. M. Burbaev, T. N. Zavaritskaya, V. A. Kurbatov, N. N. Mel'nik, V. A. Tsvetkov, K. S. Zhuravlev, V. A. Markov, and A. I. Nikiforov, Semiconductors **35**, 941 (2001).

46. V. Ya. Aleshkin and N. A. Bekin, J. Phys.: Condens. Matter **9**, 4841 (1997).

47. M. L. W. Thewalt, D. A. Harrison, C. F. Reinhart, J. A. Wolk, and H. Lafontaine, Phys. Rev. Lett. **79**, 269 (1997).

48. B. V. Kamenev, L. Tsybeskov, J. Baribeau, and D. J. Lockwood, Phys. Rev. B **72**, 193306 (2005).

49. M. Larsson, A. Elfving, W.-X. Ni, G. V. Hansson, and P. O. Holtz, Phys. Rev. B **73**, 195319 (2006).

50. B. Julsgaard, P. Balling, J. L. Hansen, A. Svane, and A. N. Larsen, Appl. Phys. Lett. **98**, 093101 (2011).

51. G. Bremond, M. Serpentini, A. Souifi, G. Guillot, B. Jacquier, M. Abdallah, I. Berbezier, and B. Joyce, Microelectron. J. **30**, 357 (1999).

52. W.-H. Chang, A. T. Chou, W. Y. Chen, H. S. Chang, T. M. Hsu, Z. Pei, P. S. Chen, S. W. Lee, L. S. Lai, S. C. Lu, and M.-J. Tsai, Appl. Phys. Lett. **83**, 2958 (2003).

53. D. N. Lobanov, A. V. Novikov, K. E. Kudryavtsev, D. V. Shengurov, Yu. N. Drozdov, A. N. Yablonskii, V. B. Shmagin, Z. F. Krasil'nik, N. D. Zakharov, and P. Werner, Semiconductors **43**, 313 (2009).

54. L. V. Asryan and S. Luryi, Solid State Electron. **47**, 205 (2003).

55. D.-S. Han, and L. V. Asryan, Appl. Phys. Lett. **92**, 251113 (2008).

Translated by A. Kazantsev